Available online at www.sciencedirect.com
ScienceDirect
Developmental Biology 304 (2007) 317–325
DEVELOPMENTAL BIOLOGY
www.elsevier.com/locate/ydbio

Oocyte CD9 is enriched on the microvillar membrane and required for normal microvillar shape and distribution

Kathryn E. Runge [a], James E. Evans [a], Zhi-Yong He [a], Surabhi Gupta [a], Kent L. McDonald [b], Henning Stahlberg [a], Paul Primakoff [c,*], Diana G. Myles [a]

[a] Section of Molecular and Cellular Biology, University of California Davis, Davis, CA 95616, USA
[b] Electron Microscope Laboratory, University of California, Berkeley, CA 94720, USA
[c] Department of Cell Biology and Human Anatomy, School of Medicine, University of California Davis, Davis, CA 95616, USA

Received for publication 25 October 2006; revised 15 December 2006; accepted 18 December 2006
Available online 23 December 2006

Abstract

Microvilli are found on the surface of many cell types, including the mammalian oocyte, where they are thought to act in initial contact of sperm and oocyte plasma membranes. CD9 is currently the only oocyte protein known to be required for sperm–oocyte fusion. We found CD9 is localized to the oocyte microvillar membrane using transmission electron microscopy (TEM). Scanning electron microscopy (SEM) showed that CD9 null oocytes, which are unable to fuse with sperm, have an altered length, thickness and density of their microvilli. One aspect of this change in morphology was quantified using TEM by measuring the radius of curvature at the microvillar tips. A small radius of curvature is thought to promote fusibility and the radius of curvature of microvillar tips on CD9 wild-type oocytes was found to be half that of the CD9 null oocytes. We found that oocyte CD9 co-immunoprecipitates with two Ig superfamily *cis* partners, EWI-2 and EWI-F, which could have a role in linking CD9 to the oocyte microvillar actin core. We also examined latrunculin B-treated oocytes, which are known to have reduced fusion ability, and found altered microvillar morphology by SEM and TEM. Our data suggest that microvilli may participate in sperm–oocyte fusion. Microvilli could act as a platform to concentrate adhesion/fusion proteins and/or provide a membrane protrusion with a low radius of curvature. They may also have a dynamic interaction with the sperm that serves to capture the sperm cell and bring it into close contact with the oocyte plasma membrane.

Keywords: Fertilization; Microvilli; CD9; Tetraspanin

Introduction

The surface of the mammalian oocyte can be divided into two regions. The larger region is covered with a dense population of microvilli, while the smaller region lacks microvilli. Sperm binding and fusion have been reported to be restricted to the microvilli-rich region of the oocyte, indicating the importance of this domain of the plasma membrane for sperm–oocyte fusion (Yanagimachi, 1978).

Microvilli are a surface feature of many cell types. They serve a diverse set of functions, from increasing absorptive surface area in the epithelial brush border to the mechanosensitive reception of hair cells of the inner ear (Heintzelman and Mooseker, 1992; Roberts et al., 1988). Relevant to this study, microvilli have also been shown to participate in cell–cell adhesion during tethering of leukocytes. For successful leukocyte tethering to the surface of endothelial cells, the leukocyte adhesion protein L-selectin must be restricted to microvillar membranes (Ivetic et al., 2004).

Images of sperm–oocyte fusion, from both TEM and SEM studies, have implicated oocyte microvilli in the fusion process. Scanning electron micrographs of mammalian oocytes show the sperm being enveloped by the oocyte microvilli during fusion while transmission electron micrographs suggest that the sperm fuses first with the microvilli and not with the planar membrane region between microvilli (Shalgi and Phillips, 1980; Yanagimachi and Noda, 1970).

In addition to microvilli, other actin-based protrusions are found on the surface of cells. In non-mammalian fertilization, such actin-based protrusions have been shown to play a role by localizing

* Corresponding author.
E-mail address: pdprimakoff@ucdavis.edu (P. Primakoff).

0012-1606/$ - see front matter © 2006 Elsevier Inc. All rights reserved.
doi:10.1016/j.ydbio.2006.12.041

adhesion molecules to the acrosomal process of sea urchin sperm and of fusion molecules to the fertilization tubule of the mt+ *Chlamydomonas* gamete (Longo et al., 1994; Misamore et al., 2003; Monroy, 1985).

We have used two approaches to investigate the role of oocyte microvilli in mouse sperm–oocyte fusion. First we asked if CD9, an oocyte surface protein required for gamete fusion, was localized to the microvillar membrane. It has been shown by immunofluorescence that expression of CD9 is localized to the microvilli-rich region of the oocyte (Kaji et al., 2000). Here we studied the distribution of CD9 within the microvilli-rich region. We also asked if oocyte CD9 is associated with the Ig super-family (IgSF) proteins EWI-2 and EWI-F. These two IgSF molecules may serve as linkers between surface proteins and ezrin, radixin and moesin (ERM proteins), which in turn bind to the actin core of microvilli (Sala-Valdes et al., 2006).

We also investigated oocytes that were impaired in their ability to fuse with sperm to determine if they had an altered microvillar distribution or microvillar shape. We examined oocytes from CD9 knockout mice which have lost their ability to fuse with sperm (Kaji et al., 2000; Le Naour et al., 2000; Miyado et al., 2000). We also examined oocytes treated with latrunculin B with the aim of directly affecting microvillar structure. Latrunculin B inhibits microfilament polymerization by sequestering monomeric actin and latrunculin B-treated oocytes had previously been shown to have reduced fusion ability (McAvey et al., 2002).

In this study we found that CD9 is primarily localized to the membrane of the microvilli and sparse in the planar region between the microvilli. CD9 on oocytes associates with two CD9 cis partners, EWI-2 and EWI-F, which have a role of linking CD9 to ERM proteins and hence the microvillar actin core. We also documented an alteration in the structure and number of microvilli on fusion-deficient oocytes. Our results are consistent with CD9 localization and normal microvillar size, shape and density on the egg membrane being required for sperm–egg fusion.

Materials and methods

Gamete isolation

Wild-type ICR or C57BL/6 (Charles River, Wilmington, MA) female mice, 6–8-week-old, were used for oocyte collection. Oocytes lacking CD9 were collected from CD9 null mice (a gift from Dr. Claude Boucheix, INSERM, Villejuif, France). To obtain zona pellucida-free oocytes, females were super-ovulated, oocytes were collected and adherent cumulus cells were released as described previously (Yuan et al., 1997). To loosen the zona pellucida (ZP), the oocytes were treated with 30 μg/ml chymotrypsin (Sigma-Aldrich, St. Louis, MO) for 3 min at 37 °C and 5% CO_2 in medium M199 (Invitrogen, Carlsbad, CA) containing 3.5 mM sodium pyruvate (Sigma-Aldrich), and 1000 IU of penicillin–streptomycin (Invitrogen) (M199*). The zonae pellucidae were then removed mechanically using a narrow bore pipette. The oocytes were washed through three 100-μl drops of fresh M199* at which point they were ready for preparation for imaging. Wild-type ICR mice were used in many experiments as they were comparable to wild-type C57BL/6 in microvillar structure and ovulated a greater number of oocytes.

Scanning electron microscopy (SEM)

Oocytes from wild-type and CD9 knockout mice were isolated as above and fixed in 2.5% glutaraldehyde (Sigma-Aldrich) and 1× Brinkley Buffer 80 (BRB80) (Desai et al., 1999) in M199*. After fixation overnight at 4 °C, the oocytes were transferred into double distilled water and dehydrated through a graded series of acetones. Following washing with 100% ethanol, the oocytes were dried in a Samdri 780A critical point drying apparatus and were transferred onto a stub with carbon tape, and coated with gold in a Denton Vacuum Desk II sputter coater. A Hitachi S3500N scanning electron microscope was used for imaging.

SEM of treated oocytes

ZP-free oocytes were retrieved as described above and incubated with 4 μg/ml latrunculin B (VWR, Brisbane CA) or 0.5% DMSO in M199* for 1 h at 37 °C in 5% CO_2. They were then washed through four 100 μl drops of M199* and prepared as described above for imaging by SEM.

Transmission electron microscopy (TEM)

Cells were fixed as for SEM, washed through four 100 μl drops of double distilled water, then postfixed in 1% OsO_4 (Ted Pella, Redding CA) for 1 h. After postfixation, oocytes were stained overnight in 1% aqueous uranyl acetate (UA). Samples were dehydrated through a graded series of acetones, infiltrated with 50% eponate araldite resin (Ted Pella) in acetone, infused three times in pure resin and polymerized 48 h at 60 °C. 70 nm sections were prepared and stained with lead citrate and UA. Sections were examined on a Philips 410 electron microscope or Philips CM120. Images were captured by the Digital Micrograph imaging system.

Immunoelectron microscopy on oocytes

After isolation and ZP removal, oocytes were fixed in 4% paraformaldehyde, and labeled using a monoclonal antibody against CD9 (KMC8) (1:200 in M199*; BD Pharmingen, Palo Alto, CA) for 1 h, washed through four 100 μl drops of M199* and then labeled with a 10 nm gold-conjugated anti-rat IgG secondary antibody (Ted Pella #15771) for 30 min and washed through four 100 μl drops of M199*. Samples were then prepared for TEM as described above. Some samples were first labeled with primary and secondary antibodies, followed by fixation.

Electron tomography

Immunolabeled samples were cut into 100–200 nm thick sections by ultramicrotomy and were subsequently visualized on a JEM-2100F field emission gun transmission electron microscope operating at 200 keV. Images were recorded on a 2048×2048 pixel Tietz Video Image Processing CCD camera with a nominal magnification of 24,000× and a defocus of ~2 microns. Two perpendicular tilt-series (in-plane) of the same section were acquired in one degree increments from −60 to +60 degrees. Data from two orthogonal tilt-series were aligned utilizing the 10 nm gold particles as fiducial markers to precisely determine the exact tilt angle, skew and magnification of each 2-D projection image with the IMOD software package (Mastronarde, 1997). The aligned tilt-series were then combined to generate a 3-D reconstruction of the volume using a weighted back-projection algorithm and filtered for better visualization using a bilateral denoising algorithm (Jiang et al., 2003). The tomogram was then analyzed and modeled as surface renderings to localize the outer-membrane and the immunolabeled gold (Kremer et al., 1996).

Calculations of membrane length, molecular distribution and microvillar curvature

Measurements of microvillar and planar membrane length were taken from TEM images using Scion Image. Counts of gold particles were taken from these images and the number of gold particles recorded as either being on the measured planar membrane or measured microvillar membrane. Radius of curvature at the tips of microvilli was determined by analyzing these same images using PhotoShop. Radius of curvature was determined to be the radius of a circle which fits the curve at the tip of the microvillus. Only microvilli with distinct tips were used. Twenty-five microvilli were measured for both CD9 wild-type and CD9 null oocytes.

Production of CD9 partners EWI-2 and EWI-F and antisera to these proteins

Mouse EWI-2 cDNA was amplified by PCR from mouse heart cDNA (Clonetech). The primers used for this reaction were EWI-2F (AAGATC-TATGGGCGTCCCTAGCCCCACG) and EWI-2R (aagagctcccactctaggt-gatggctgg). The coding region for the EWI-2 extracellular domain (EWI-2EC) was then amplified from EWI-2 full-length cDNA by two primers: EWI-2F and EWI-2ec (aactcgagcacaaataggtatccacagc). EWI-2EC was placed in a baculo-virus express system transfer vector (termed pFB-MH, a C-terminal myc-His tags donor vector derived from pFastBac1, constructed in our lab). Recombinant baculovirus containing EWI-2EC coding sequence was obtained by following the baculovirus system protocol (Invitrogen). Recombinant EWI-2EC was purified from infected Sf9 cell supernatant using a Ni-CAM resin column (Sigma). SDS-PAGE, followed by silver staining of 100 ng of purified protein, showed a single band migrating as expected for EWI-2EC and no contaminating bands. Antisera against the EWI-2 extracellular domain were raised by injecting purified EWI-2EC into rabbits. For immunofluorescent detection of EWI-2 on the oocyte surface, a 1:100 dilution of antiserum was used, followed by anti-rabbit IgG conjugated to AlexaFluor 488 (Molecular Probes). Control oocytes were incubated with a 1:100 dilution of pre-immune serum.

The entire extracellular portion of mouse EWI-F cDNA (bases 1–2490) was PCR amplified using primers EWIF-F: 5′-CCTCAGACCGAGCATGGGGCG-3′ and EWIF-R: 5′-tcagcacgtccatcttcacagtta-3′. The PCR product was cloned into pcDNA3.1/V5-His-TOPO vector (Invitrogen) following the manufacturer's instructions. The resulting plasmid was transfected into CHO cells using Lipofectamine 2000 (Invitrogen). Soluble recombinant EWI-F protein was purified from the spent media using Ni^{+2}-agarose beads (Qiagen). The protein was eluted with 250 mM imidazole (Sigma) and concentrated using centriprep YM-10 (Millipore). Silver staining of 10ug of purified protein per lane in SDS-PAGE revealed only one trace contaminant. The concentrated protein was dialyzed extensively against PBS and used as an immunogen to generate antisera in guinea pigs. For immunofluorescent detection of EWI-F on the oocyte surface, a 1:50 dilution of antiserum was used, followed by anti-guinea pig IgG conjugated to AlexaFluor 488 (Molecular Probes). Control oocytes were incubated with a 1:50 dilution of pre-immune serum.

Immunoprecipitation of CD9

Cumulus-free, zona intact oocytes were collected from 100 female ICR mice as described above in M199* containing 0.4% polyvinylalcohol (PVA). All oocytes were pooled into 1 ml of PBS + 0.4% PVA on a culture dish and washed three times through 1 ml of PBS/0.4% PVA on culture dishes. The oocytes were then transferred to 200 μl of PBS lacking PVA, then again to 100 μl and finally to 50 μl. Since the oocytes are a precious resource, they were used in two sequential experiments. After release of GPI-anchored proteins (for an unrelated study), oocytes were washed and lysed in 100 μl HBS + 1% Brij97 for 30 min at 4 °C in the presence of protease inhibitors. Insoluble material was removed by centrifugation at 14,000 rpm for 10 min at 4 °C and the lysate was stored at −80 °C. This complete procedure was performed seven times and over 14,000 oocytes were obtained, lysed and the lysate frozen.

Lysates were thawed on ice, pooled and incubated for 3 h at 4 °C with 20 μl agarose bead slurry coupled to KMC8 mAb (Pharmingen). The beads were removed by centrifugation at 5000 rpm for 5 min at 4 °C and stored on ice. The pooled lysates were incubated for anoth er 3 h at 4 °C with an additional 20 μl of KMC8-coupled beads, which were then removed by centrifugation and pooled with the previous beads. The pooled beads were washed with 200 μl HBS + 1% Brij97 five times and resuspended in 20 μl of 1× non-reducing SDS sample buffer.

Analysis of the immunoprecipitate

The immunoprecipitate in 20 μl of SDS-PAGE sample buffer was heated at 96 °C for 10 min. Separation of CD9 and its partners was carried out by SDS-PAGE (4–20% gel) under non-reducing conditions. The dye front was run 4 cm down the gel after which the gel was stained using Colloidal Coomassie Blue for 5 h at room temperature. Destaining was carried out overnight at room temperature. The sample lane was excised and cut into 5 pieces (< 1 cm^2). The pieces were placed into sterile 1.5 ml centrifuge tubes and washed twice with 1 ml of 50% acetonitrile. The samples were stored at −20 °C. Proteolytic digestion and mass spectrometric analysis of the samples were performed at the Harvard Microchemistry Facility by microcapillary reverse-phase HPLC nano-electrospray tandem mass spectrometry (μLC/MS/MS) on a Finnigan LCQ DECA XP Plus quadrupole ion trap mass spectrometer. Interpretation of the results was provided by the Harvard Microchemistry Facility and was additionally evaluated by a manual protein BLAST search of the NCBI protein database.

Results

CD9 is expressed on mouse oocyte microvilli

The mature mouse oocyte plasma membrane is divided into two large subdomains. The region over the metaphase arrested chromosomes has a relatively smooth surface. The rest of the oocyte is covered with microvilli and is the "microvilli-rich region" where sperm bind and fuse (Fig. 1). CD9 has been found by immunofluorescence to be enriched on the microvilli-rich domain of the oocyte (Kaji et al., 2000). To determine the relationship of CD9 to the microvilli, we examined wild-type oocytes labeled with a monoclonal antibody to CD9 (KMC8) and a colloidal gold conjugated secondary antibody. The majority of CD9 molecules were congregated on the microvilli

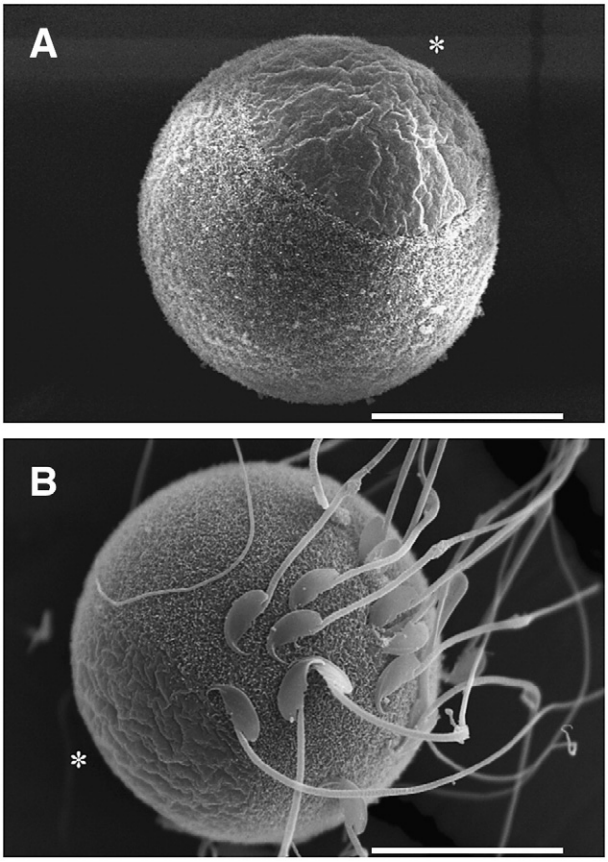

Fig. 1. Sperm bind to the region of the oocyte with a high concentration of microvilli. (A) Wild-type oocyte showing microvilli-free (*) and microvilli-rich regions. (B) Wild-type oocyte after incubation with sperm for 25 min. Sperm are not bound to microvilli free region. Scale bars, 20 μm.

and not on the planar membrane regions in between the microvilli. This was true whether the cells were labeled before fixation (Fig. 2A) or after fixation with paraformaldehyde (Fig. 2B). No gold particles were bound to wild-type oocytes labeled with only the gold-conjugated secondary antibody and no KMC8 (Fig. 2C). Also CD9 null oocytes labeled with KMC8 and gold-conjugated secondary antibody exhibited no gold particles (data not shown).

However, as individual 2-D electron micrographs are projections of the entire section, it was difficult in some cases to assign a gold particle to either membrane. Therefore, we utilized electron tomography to obtain a more complete representation of the localization of CD9 on the oocyte surface. This technique allowed for the visualization of a 3-D volume of each microvillus and clear determination of CD9 distribution along the entire microvillar membrane. This was achieved by acquiring dual-axis tilt series for several 100–200 nm thick sections of oocyte microvilli. These data sets were aligned and back-projected to reconstruct 3-D tomograms which could be modeled and analyzed. The tomogram reproduced in Fig. 2D shows immunolabeled molecules spread along the microvillus with a tendency to localize at the tip.

We then quantified this distribution with TEM by measuring the lengths of the planar membranes and of microvillar membranes from the images, and counting the bound gold particles. The number of gold particles per linear micron of membrane was calculated from these measurements (Fig. 2E). Calculations were done using oocytes prefixed in paraformaldehyde before antibody labeling to prevent antibody-induced changes in CD9 distribution. The concentration of CD9 molecules on microvillar membrane was found to be in average ~4 times greater than that on the planar membrane (Fig. 2E).

Deletion of CD9 results in altered microvillar morphology

To determine if deleting CD9 altered microvillar morphology, we examined oocytes from CD9 knockout mice by both SEM and TEM. SEM images showed that on CD9 KO oocytes the distribution of microvilli was quite dense compared to wild-type oocytes. Fig. 3 shows the microvilli of a representative wild-type oocyte (Fig. 3A) and a representative CD9 null oocyte (Fig. 3B). A qualitative, visual assessment of the density of the microvilli from images of these two types of oocytes is shown in Table 1 and it indicates that CD9 knockout oocytes show denser arrays of microvilli than wild-type oocytes.

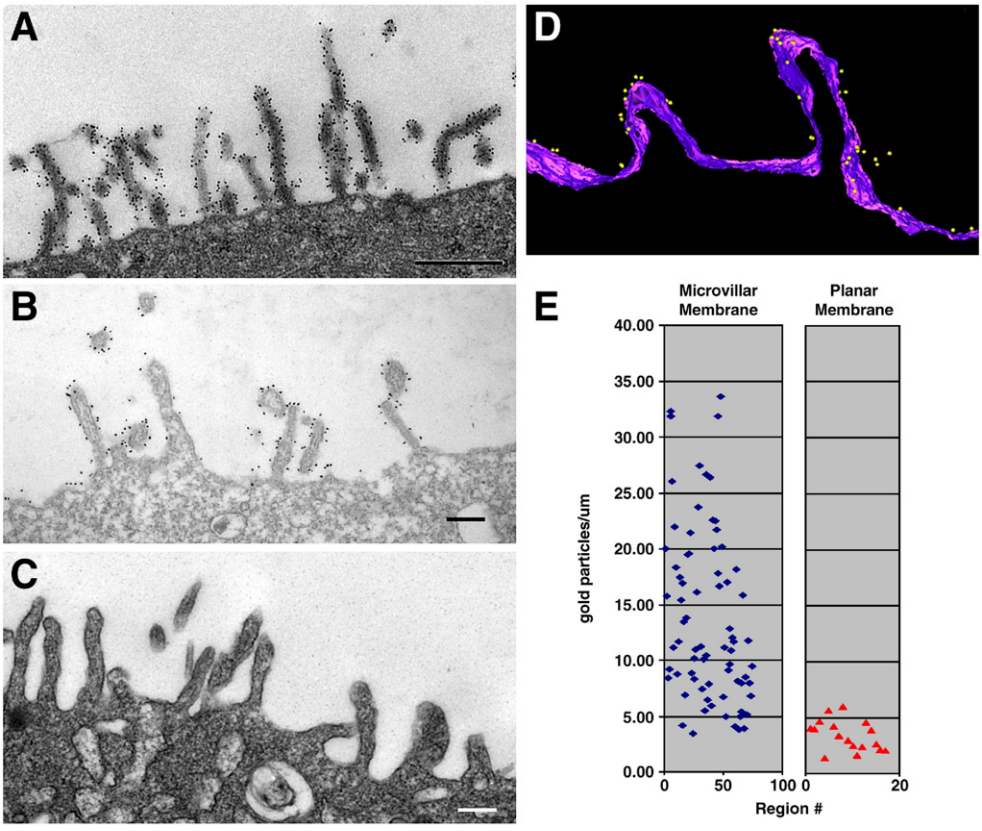

Fig. 2. Localization of CD9 to individual microvilli. (A) Electron micrograph of wild-type oocyte labeled live for CD9 with no prefixation (scale bar, 0.5 μm). (B) Electron micrograph of wild-type oocyte labeled for CD9 with paraformaldehyde prefixation (scale bar, 0.2 μm). (C) Electron micrograph of wild-type oocyte labeled with only gold-conjugated secondary antibody (scale bar, 0.2 μm). (D) Representative model generated from a 3-D tomogram of wild-type oocyte labeled for CD9. Oocyte plasma membrane is depicted in magenta and CD9 molecules as yellow spheres. (E) Distribution plot of number of gold particles per linear micron of sectioned planar membrane versus microvillar membrane. Each blue diamond represents a region of microvillar membrane and each red triangle represents a region of planar membrane.

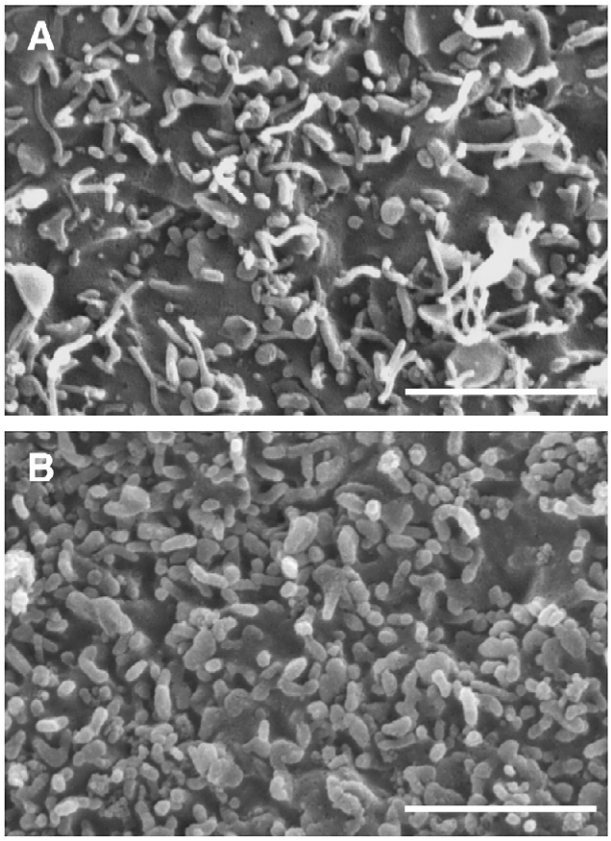

Fig. 3. Altered membrane structure in fusion deficient oocytes. SEM of the surface of unfertilized mouse oocytes with the zona pellucida removed. Images taken at 20K magnification. Scale bars, 2 μm. (A) Wild-type; (B) CD9-KO.

CD9 null microvilli (Fig. 3B) appeared uniformly short and thick; in comparison wild-type oocytes displayed microvilli with a variety of shapes, including many that were long and thin (Fig. 3A). Related results were obtained when oocytes were visualized by TEM (Fig. 4). In some cases, the thickness of a microvillus on CD9 KO oocytes was twice that of the average microvillus of wild-type oocytes (Figs. 4A and B). Long microvilli were occasionally found in micrographs of wild-type oocytes, but were not observed on oocytes from CD9 knockout mice.

CD9 null oocytes have altered radius of curvature of the microvilli

We asked if the change in microvillar morphology had an effect on the radius of curvature of the microvillar tip. Only microvilli with a distinct, plasma membrane bounded terminus were used for this calculation; microvilli were excluded from the measurements if the tip was blurred suggesting a bend out of the plane of section. When wild-type microvillar tips were compared to CD9 KO microvillar tips, it was found that the radius of curvature at the microvillus tip of CD9 KO oocytes was close to two fold higher than on wild-type oocytes (Fig. 4C).

Transmembrane microvillus linker proteins are in a complex with CD9 on oocytes

The cellular parameters that regulate microvillar shape, size and density are uncertain and the role of CD9 in microvillar morphology is unknown (Gorelik et al., 2003; Okumura et al., 2001). In tissue culture cells, several labs have found that CD9 has a tight, direct association with the IgSF proteins EWI-2 and EWI-F (Charrin et al., 2001; Stipp et al., 2001a,b). EWI-2 and EWI-F cytoplasmic tails bind to the N-terminus of ezrin or moesin (Sala-Valdes et al., 2006). Ezrin, radixin and moesin (ERM) proteins at their C-terminus bind to the actin filaments in microvilli and other cellular protrusions (Turunen et al., 1994). Thus, the EWI proteins and ERM proteins form a linker system from CD9 on the surface to the internal actin cytoskeleton in tissue culture cells and this system may have a role in microvillar morphology, dynamics or function. To determine if oocytes have a similar network of proteins interacting with CD9, we made antibodies to purified, recombinant EWI-2 and EWI-F and found that these antibodies bind to the surface of oocytes (Fig. 5). Furthermore when CD9 was immunoprecipitated from an oocyte lysate, among the co-precipitating proteins identified, after SDS-PAGE and mass spectrometry, were both EWI-2 and EWI-F (Table 2).

Effect of latrunculin B on microvillar morphology

Finally to test a small molecule inhibitor, we used latrunculin B which has been shown to inhibit sperm–oocyte fusion (McAvey et al., 2002). Latrunculins sequester actin monomers (Spector et al., 1989) and would therefore be predicted to affect microvilli. Oocytes treated with latrunculin B showed a dramatic change in microvillar morphology as observed by SEM and TEM (Fig. 6). In SEM, some oocytes showed either a complete lack of microvilli, or small patches of microvilli surrounded by smooth membrane (Fig. 6A). The DMSO control was similar to untreated oocytes (Fig. 6B). Latrunculin B-treated oocytes, viewed by TEM, also showed few to no microvilli around the periphery of the oocyte (Fig. 6D). Oocytes treated with latrunculin B, when processed for EM, developed numerous blebs, except in one region about the size of the microvillar free region (Fig. 6C). The blebs may be a reagent-induced alteration in the sensitivity of the membrane to the fixation process causing artifactual blebbing.

Discussion

We have observed two aspects of oocyte microvilli that suggest a role for these structures during fusion between the oocyte and the sperm. First, we have documented the

Table 1
Visual assessment of SEM images showing density of microvilli on surface of wild-type and CD9 null oocytes

Density of microvilli	WT ($n=65$)	CD9 null ($n=33$)
Dense	16%	75%
Medium dense	43%	24%
Sparse	41%	1%

n=total number of oocytes in which images were scored.

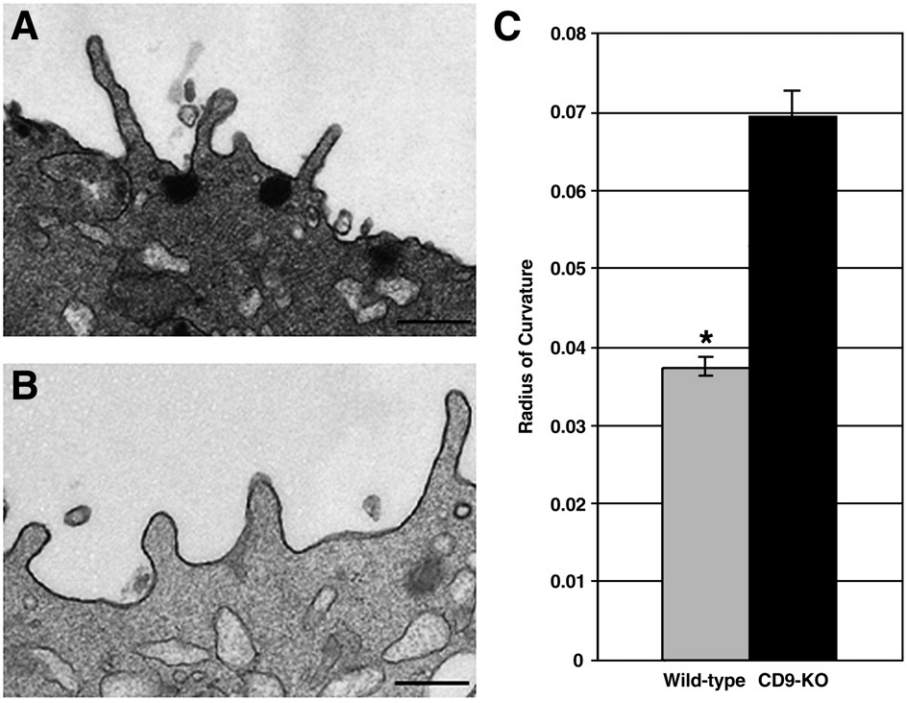

Fig. 4. Increase in radius of curvature of microvillar tips in CD9-KO oocytes. (A–B) TEM images of microvilli of unfertilized mouse oocytes with the zona pellucida removed (scale bars, 0.5 μm). (A) Wild-type; (B) CD9 KO; (C) Measurements of curvature were taken at the tips of microvilli represented in cross-sectional TEM images of wild-type, and CD9 knockout oocytes, like those in panels A and B. Data represent the mean value ± SE of microvillar tips from $n = 25$ wild-type and $n = 25$ CD9 KO oocytes, $*p < 0.05$.

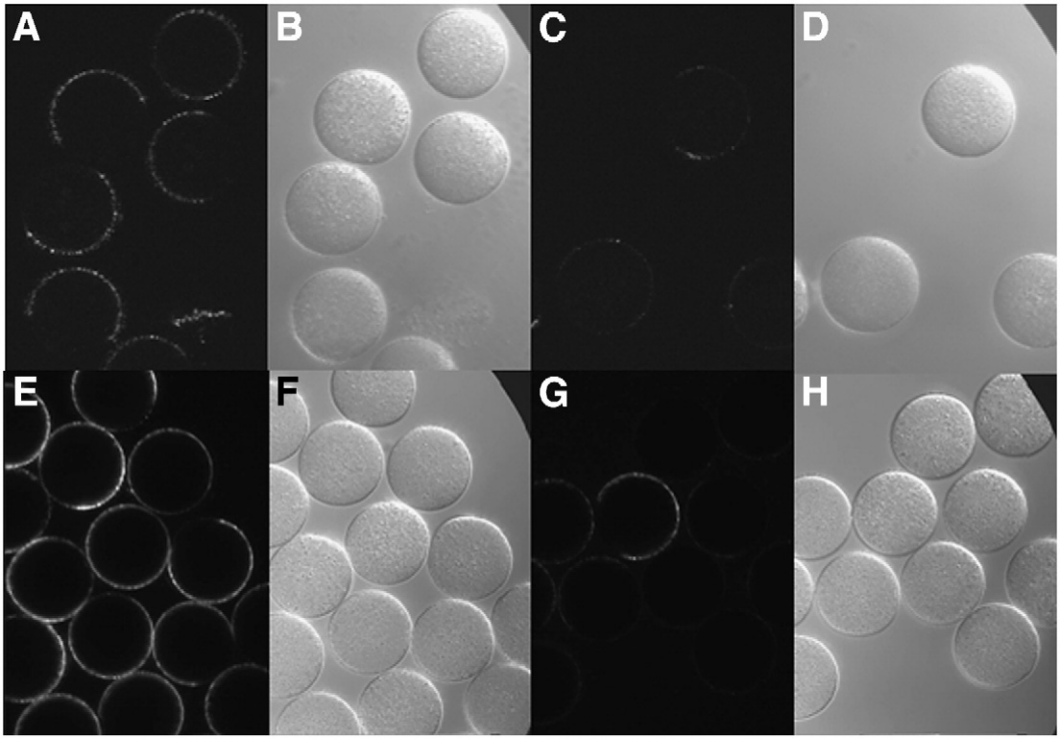

Fig. 5. Immunofluorescent staining of oocytes with anti-EWI-F and anti-EWI-2 antibodies. (A–B) Anti-EWI-F antiserum staining and phase contrast of same oocytes. (C–D) Pre-immune serum staining and phase contrast of same oocytes. (E–F) Anti-EWI-2 antiserum staining and phase contrast of same oocytes. (G–H) Pre-immune serum staining and phase contrast of same oocytes. Clear surface staining is observed on each oocyte using either anti-EWI-F or anti-EWI-2 antibodies. Staining with the control, pre-immune antisera is negative except for one weakly stained oocyte in panel G.

Table 2
Identification by mass spectrometry of CD9 and two other proteins that co-precipitate with CD9 in an oocyte-lysate

Peptide fragment sequence	Closest protein match
LDTVGSDAYR VLADALVVGPSSRPPPGLSLR VDGVVLEK KTPDTSLLASHMLAR EGEPFELR	EWI-F (prostaglandin F2 receptor negative regulator)
LVAQLDTEGIGSKGPGYEDR SDMAVEAGAPYAER	EWI-2 (Ig super family receptor PGRL)
ELQEFYKDTTYQK SKDEPQRETLK	CD9

localization of CD9 to the microvillar membrane. Additionally, we found a correlation between the loss of fusion ability of oocytes and alteration in the morphology of their microvilli.

The finding that CD9, an oocyte protein required for gamete fusion, is concentrated on the oocyte microvilli has several potential implications. One possibility is that the microvilli concentrate CD9 molecules in a site that initially contacts the sperm (Yanagimachi et al., 1973). In other cell types, concentration of cell–cell adhesion molecules has been found on microvilli. L-selectin on lymphocytes and l-gicerin on fibroblasts are both involved in cell adhesion and are localized to microvillar structures (Ivetic et al., 2004; Okumura et al., 2001). It has also been shown in *Chlamydomonas* and the sea urchin that important fertilization molecules are localized to the membrane of actin-based protrusions where fusion occurs. *Chlamydomonas* concentrates the fusion-related molecule Fus1 to the tip surface of its mt+ fertilization tubule (Misamore et al., 2003) and the sea urchin sperm–oocyte adhesion protein bindin is concentrated on the surface of the sperm acrosomal process (Longo et al., 1994). Similar to these examples, localization of CD9 within the microvillar membrane subdomain increases CD9 surface density, which could control the adhesive/fusogenic properties of the membrane.

Another possibility is that localization of the tetraspanin CD9 reflects a participation of the tetraspanin web in the formation or maintenance of the microvillar structure. The tetraspanin web is a network of interacting proteins on the cell surface organized by various tetraspanins, including CD9 (Hemler, 2003; Levy and Shoham, 2005; Rubinstein et al., 1996). The activities of microvilli depend on a functional attachment of surface proteins to the internal actin cytoskeleton in the microvillus (Bartles, 2000; Fath and Burgess, 1995). While CD9 is known to associate with various other plasma membrane proteins on a CD9-expressing cell, among the most stable CD9 partners are the novel IgSF proteins EWI-2 and EWI-F that belong to a small IgSF subfamily (Charrin et al., 2001; Stipp et al., 2001a,b). According to current findings, EWI-2 and EWI-F bind directly to ERM (ezrin, radixin and moesin) proteins through their cytoplasmic tails. The EWI proteins can also bind indirectly to ERM by lateral association with their tetraspanin partner CD81 which binds to ERM (Sala-Valdes et al., 2006). Another recent report shows that CD9 in cell–cell contact sites is laterally associated with I-CAM-1 or V-

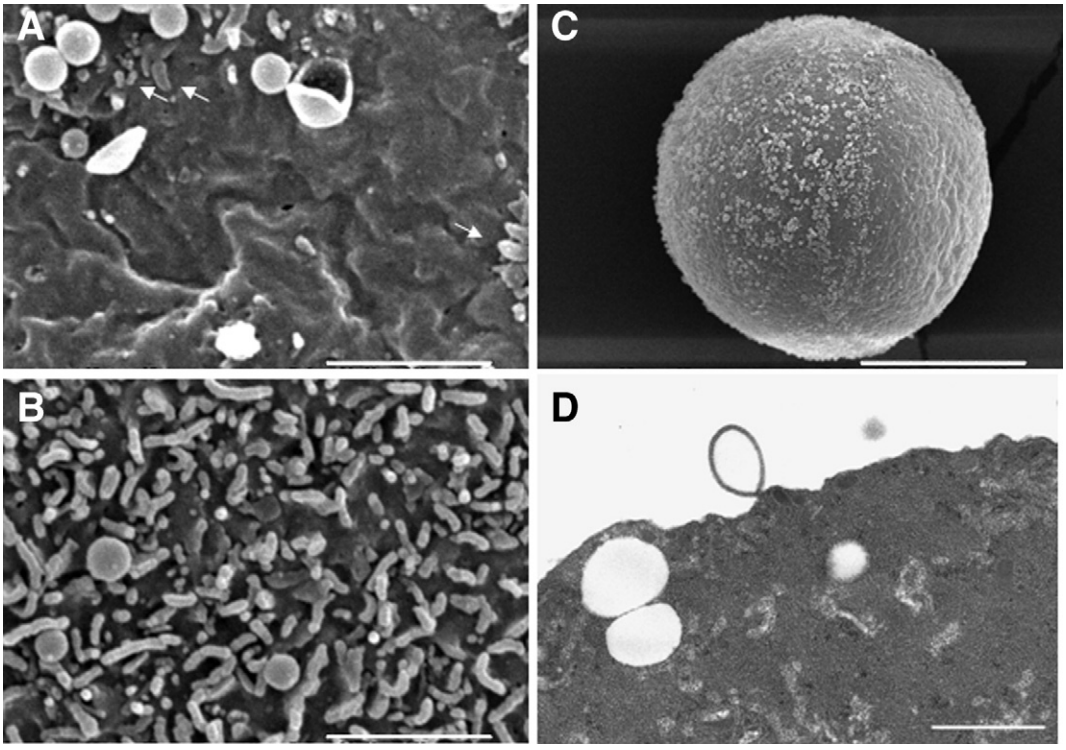

Fig. 6. Oocytes treated with latrunculin B lose most of the microvilli on the plasma membrane. SEM images of oocytes treated with: (A) latrunculin B and (B) 0.5% DMSO (solvent) (scale bars, 2 μm). Arrows show rare remaining microvilli after latrunculin B treatment. (C) Lower magnification SEM view of latrunculin B-treated oocyte, showing distribution of blebs (scale bar, 20 μm). (D) TEM of latrunculin B-treated oocyte (scale bar, 1 μm). All microvilli are apparently absent from the TEM image of treated oocytes while a few remain in the SEM image (A) with severe blebbing of membrane.

CAM-1, each of which is an IgSF protein that can intracellularly bind to ERM proteins (Barreiro et al., 2005). ERM proteins in turn bind to the actin filaments of the microvillar core (Turunen et al., 1994). These studies in tissue culture cells define a network of proteins that attach CD9 on the cell surface to the actin cytoskeleton, in a CD9-IgSF-ERM-actin linkage. Using both immunofluorescence microscopy and mass spectrometry, we found that EWI-2 and EWI-F are present in oocytes and co-precipitate with CD9, suggesting a functional connection in the oocyte microvilli. In a recent review (Chen and Olson, 2005), it is proposed that cell–cell fusion in general will require appropriate deployment of the actin cytoskeleton and our findings on mouse gamete fusion are consistent with this idea. The detailed role of a possible oocyte CD9-EWI-ERM-actin network remains to be studied.

The observation that the oocytes impaired in fusion (CD9 null oocytes or oocytes treated with latrunculin B) (Kaji et al., 2000; Le Naour et al., 2000; McAvey et al., 2002; Miyado et al., 2000) also show alterations in microvillar structure, implies that the microvilli may have an important structural role in fusion. Several potential mechanisms involved in a structural role of microvilli can be considered.

First, microvilli on the oocyte surface may provide a protrusion which maximizes the efficiency of sperm fusion. It has been noted that, in several cases of cell fusion (gametes or somatic cells), a membrane projection with a small radius of curvature at the tip participates in fusion (Monroy, 1985; Wilson and Snell, 1998). It is possible that the small radius of curvature, present at the tips of the oocyte microvilli, might decrease the repulsive force caused by the hydration barrier as well as electrostatic repulsion of the negatively charged membranes (Lee et al., 2005; McMahon and Gallop, 2005; Monroy, 1985; Ostrowski et al., 2004; Zimmerberg and Kozlov, 2006). When a comparison is made between the efficiency of fusion of large unilamellar vesicles (large radius of curvature) and small unilamellar vesicles (small radius of curvature), the small vesicles fuse under conditions where the large will not (Lentz et al., 1992). A small radius of curvature is found in the membrane of the sea urchin sperm acrosomal process that is the first membrane region to interact and fuse with the oocyte plasma membrane (Longo et al., 1994; Schatten and Schatten, 1983). This is also true for the acrosomal processes of the sea cucumber, horseshoe crab and starfish (Detmers, 1985; Kyozuka and Osanai, 1988; Tilney and Inoue, 1987) as well as the fertilization tubule of the mt+ gamete in *Chlamydomonas* (Goodenough et al., 1982).

An alternate possibility is that dynamic microvilli are needed for the sperm to interact with the oocyte for fusion and subsequent engulfment. Microvilli have been shown to be "dynamic" in epithelial cells using scanning ion conductance microscopy to demonstrate that the microvilli have formation states, steady states and retraction states (Gorelik et al., 2003). The highest number of microvilli is at the steady state length, but many shorter microvilli are found, representing the transition stages of formation and retraction. We observed that microvilli on the surface of a wild-type mouse oocyte are of varying sizes and shapes, suggesting a dynamic state. Furthermore, initial sperm–oocyte contact appears to trigger localized simultaneous growth of nearby microvilli. Growth of oocyte microvilli in response to initial sperm contact has been seen in at least human, hamster and sea urchin oocytes (Bronson, 1998; Cline et al., 1983; Shalgi and Phillips, 1980). In CD9 null oocytes, we found microvilli to be largely of a uniform, short and thick shape and densely arrayed on the surface. This appearance suggests that CD9 null oocytes may lack dynamic microvilli. Dynamic microvilli could be responsible for the correct positioning of the fusing membranes in relation to each other, or they could be required for the tight apposition of the two membranes that will eventually lead to lipid bilayer confluence. Dynamic microvilli may also act in part to physically trap the sperm.

One question that arises from our findings is whether the observed changes in microvillar structure or dynamics could be sufficient to cause the dramatic inability of certain types of oocytes to fuse with sperm. In the case of CD9, loss of this protein could block gamete fusion solely because of the effect on microvilli. However, we have previously found that CD9 may associate with unidentified oocyte surface proteins (Zhu et al., 2002) and/or a sperm surface ligand (Ellerman et al., 2003) and these interactions may be required for gamete fusion. The three possibilities are not mutually exclusive and each may eventually prove to be correct.

Acknowledgments

We are grateful to Grete Adamson for advice and assistance in the sectioning of samples for the TEM, to Rick Harris for instruction and advice on SEM, TEM, and quantitative techniques and to Jowell Go for research on SEM protocols. We thank Dr. Jen Alfieri, Dr. Diego Ellerman, Dr. Katie Stein, Dr. Guo-Zhang Zhu, Arlan Martin and Jowell Go who gave their time and skill for oocyte collection for the experiments identifying CD9 partners. We are very grateful for the work done by Dr. Bill Lane and the Harvard University Microchemistry Facility in determining the identities of CD9 co-precipitating proteins. Supported by NIH grants HD-16580 and U54-29125.

References

Barreiro, O., Yanez-Mo, M., Sala-Valdes, M., Gutierrez-Lopez, M.D., Ovalle, S., Higginbottom, A., Monk, P.N., Cabanas, C., Sanchez-Madrid, F., 2005. Endothelial tetraspanin microdomains regulate leukocyte firm adhesion during extravasation. Blood 105, 2852–2861.

Bartles, J.R., 2000. Parallel actin bundles and their multiple actin-bundling proteins. Curr. Opin. Cell Biol. 12, 72–78.

Bronson, R., 1998. Is the oocyte a non-professional phagocyte? Hum. Reprod. Updat. 4, 763–775.

Charrin, S., Le Naour, F., Oualid, M., Billard, M., Faure, G., Hanash, S.M., Boucheix, C., Rubinstein, E., 2001. The major CD9 and CD81 molecular partner. Identification and characterization of the complexes. J. Biol. Chem. 276, 14329–14337.

Chen, E.H., Olson, E.N., 2005. Unveiling the mechanisms of cell–cell fusion. Science 308, 369–373.

Cline, C.A., Schatten, H., Balczon, R., Schatten, G., 1983. Actin-mediated surface motility during sea urchin fertilization. Cell Motil. 3, 513–524.

Desai, A., Verma, S., Mitchison, T.J., Walczak, C.E., 1999. Kin I kinesins are microtubule-destabilizing enzymes. Cell 96, 69–78.

Detmers, P.A., 1985. Elongation of cytoplasmic processes during gametic mating: models for actin-based motility. Can J. Biochem. Cell Biol. 63, 599–607.

Ellerman, D.A., Ha, C., Primakoff, P., Myles, D.G., Dveksler, G.S., 2003. Direct binding of the ligand PSG17 to CD9 requires a CD9 site essential for sperm–egg fusion. Mol. Biol. Cell 14, 5098–5103.

Fath, K.R., Burgess, D.R., 1995. Microvillus assembly. Not actin alone. Curr. Biol. 5, 591–593.

Goodenough, U.W., Detmers, P.A., Hwang, C., 1982. Activation for cell fusion in *Chlamydomonas*: analysis of wild-type gametes and nonfusing mutants. J. Cell Biol. 92, 378–386.

Gorelik, J., Shevchuk, A.I., Frolenkov, G.I., Diakonov, I.A., Lab, M.J., Kros, C.J., Richardson, G.P., Vodyanoy, I., Edwards, C.R., Klenerman, D., Korchev, Y.E., 2003. Dynamic assembly of surface structures in living cells. Proc. Natl. Acad. Sci. U. S. A. 100, 5819–5822.

Heintzelman, M.B., Mooseker, M.S., 1992. Assembly of the intestinal brush border cytoskeleton. Curr. Top. Dev. Biol. 26, 93–122.

Hemler, M.E., 2003. Tetraspanin proteins mediate cellular penetration, invasion, and fusion events and define a novel type of membrane microdomain. Annu. Rev. Cell Dev. Biol. 19, 397–422.

Ivetic, A., Florey, O., Deka, J., Haskard, D.O., Ager, A., Ridley, A.J., 2004. Mutagenesis of the ezrin–radixin–moesin binding domain of L-selectin tail affects shedding, microvillar positioning, and leukocyte tethering. J. Biol. Chem. 279, 33263–33272.

Jiang, W., Baker, M.L., Wu, Q., Bajaj, C., Chiu, W., 2003. Applications of a bilateral denoising filter in biological electron microscopy. J. Struct. Biol. 144, 114–122.

Kaji, K., Oda, S., Shikano, T., Ohnuki, T., Uematsu, Y., Sakagami, J., Tada, N., Miyazaki, S., Kudo, A., 2000. The gamete fusion process is defective in eggs of Cd9-deficient mice. Nat. Genet. 24, 279–282.

Kremer, J.R., Mastronarde, D.N., McIntosh, J.R., 1996. Computer visualization of three-dimensional image data using IMOD. J. Struct. Biol. 116, 71–76.

Kyozuka, K., Osanai, K., 1988. Fertilization cone formation in starfish oocytes: the role of the egg cortex actin microfilaments in sperm incorporation. Gamete Res. 20, 275–285.

Le Naour, F., Rubinstein, E., Jasmin, C., Prenant, M., Boucheix, C., 2000. Severely reduced female fertility in CD9-deficient mice. Science 287, 319–321.

Lee, M.C., Orci, L., Hamamoto, S., Futai, E., Ravazzola, M., Schekman, R., 2005. Sar1p N-terminal helix initiates membrane curvature and completes the fission of a COPII vesicle. Cell 122, 605–617.

Lentz, B.R., McIntyre, G.F., Parks, D.J., Yates, J.C., Massenburg, D., 1992. Bilayer curvature and certain amphipaths promote poly(ethylene glycol)-induced fusion of dipalmitoylphosphatidylcholine unilamellar vesicles. Biochemistry 31, 2643–2653.

Levy, S., Shoham, T., 2005. The tetraspanin web modulates immune-signalling complexes. Nat. Rev., Immunol. 5, 136–148.

Longo, F.J., Cook, S., McCulloh, D.H., Ivonnet, P.I., Chambers, E.L., 1994. Stages leading to and following fusion of sperm and egg plasma membranes. Zygote 2, 317–331.

Mastronarde, D.N., 1997. Dual-axis tomography: an approach with alignment methods that preserve resolution. J. Struct. Biol. 120, 343–352.

McAvey, B.A., Wortzman, G.B., Williams, C.J., Evans, J.P., 2002. Involvement of calcium signaling and the actin cytoskeleton in the membrane block to polyspermy in mouse eggs. Biol. Reprod. 67, 1342–1352.

McMahon, H.T., Gallop, J.L., 2005. Membrane curvature and mechanisms of dynamic cell membrane remodelling. Nature 438, 590–596.

Misamore, M.J., Gupta, S., Snell, W.J., 2003. The *Chlamydomonas* Fus1 protein is present on the mating type plus fusion organelle and required for a critical membrane adhesion event during fusion with minus gametes. Mol. Biol. Cell 14, 2530–2542.

Miyado, K., Yamada, G., Yamada, S., Hasuwa, H., Nakamura, Y., Ryu, F., Suzuki, K., Kosai, K., Inoue, K., Ogura, A., Okabe, M., Mekada, E., 2000. Requirement of CD9 on the egg plasma membrane for fertilization. Science 287, 321–324.

Monroy, A., 1985. Processes controlling sperm–egg fusion. Eur. J. Biochem. 152, 51–56.

Okumura, S., Muraoka, O., Tsukamoto, Y., Tanaka, H., Kohama, K., Miki, N., Taira, E., 2001. Involvement of gicerin in the extension of microvilli. Exp. Cell Res. 271, 269–276.

Ostrowski, S.G., Van Bell, C.T., Winograd, N., Ewing, A.G., 2004. Mass spectrometric imaging of highly curved membranes during Tetrahymena mating. Science. 305, 71–73.

Roberts, W.M., Howard, J., Hudspeth, A.J., 1988. Hair cells: transduction, tuning, and transmission in the inner ear. Annu. Rev. Cell Biol. 4, 63–92.

Rubinstein, E., Le Naour, F., Lagaudriere-Gesbert, C., Billard, M., Conjeaud, H., Boucheix, C., 1996. CD9, CD63, CD81, and CD82 are components of a surface tetraspan network connected to HLA-DR and VLA integrins. Eur. J. Immunol. 26, 2657–2665.

Sala-Valdes, M., Ursa, A., Charrin, S., Rubinstein, E., Hemler, M.E., Sanchez-Madrid, F., Yanez-Mo, M., 2006. EWI-2 and EWI-F link the tetraspanin web to the actin cytoskeleton through their direct association with ERM proteins. J. Biol. Chem.

Schatten, G., Schatten, H., 1983. Fertilization and early development of sea urchins. Scan Electron Microsc. 1403–1413.

Shalgi, R., Phillips, D.M., 1980. Mechanics of in vitro fertilization in the hamster. Biol. Reprod. 23, 433–444.

Spector, I., Shochet, N.R., Blasberger, D., Kashman, Y., 1989. Latrunculins-novel marine macrolides that disrupt microfilament organization and affect cell growth: I. Comparison with cytochalasin D. Cell Motil. Cytoskeleton 13, 127–144.

Stipp, C.S., Kolesnikova, T.V., Hemler, M.E., 2001a. EWI-2 is a major CD9 and CD81 partner and member of a novel Ig protein subfamily. J. Biol. Chem. 276, 40545–40554.

Stipp, C.S., Orlicky, D., Hemler, M.E., 2001b. FPRP, a major, highly stoichiometric, highly specific CD81- and CD9-associated protein. J. Biol. Chem. 276, 4853–4862.

Tilney, L.G., Inoue, S., 1987. Flagellar gyration and midpiece rotation during extension of the acrosomal process of Thyone sperm: how and why this occurs. J. Cell Biol. 104, 407–415.

Turunen, O., Wahlstrom, T., Vaheri, A., 1994. Ezrin has a COOH-terminal actin-binding site that is conserved in the ezrin protein family. J. Cell Biol. 126, 1445–1453.

Wilson, N.F., Snell, W.J., 1998. Microvilli and cell–cell fusion during fertilization. Trends Cell Biol. 8, 93–96.

Yanagimachi, R., 1978. Sperm–egg association in animals. Curr. Top. Dev. Biol. 12, 83–105.

Yanagimachi, R., Noda, Y.D., 1970. Ultrastructural changes in the hamster sperm head during fertilization. J. Ultrastruct. Res. 31, 465–485.

Yanagimachi, R., Nicolson, G.L., Noda, Y.D., Fujimoto, M., 1973. Electron microscopic observations of the distribution of acidic anionic residues on hamster spermatozoa and eggs before and during fertilization. J. Ultrastruct. Res. 43, 344–353.

Yuan, R., Primakoff, P., Myles, D.G., 1997. A role for the disintegrin domain of cyritestin, a sperm surface protein belonging to the ADAM family, in mouse sperm–egg plasma membrane adhesion and fusion. J. Cell Biol. 137, 105–112.

Zhu, G.Z., Miller, B.J., Boucheix, C., Rubinstein, E., Liu, C.C., Hynes, R.O., Myles, D.G., Primakoff, P., 2002. Residues SFQ (173–175) in the large extracellular loop of CD9 are required for gamete fusion. Development 129, 1995–2002.

Zimmerberg, J., Kozlov, M.M., 2006. How proteins produce cellular membrane curvature. Nat. Rev., Mol. Cell Biol. 7, 9–19.